Curriculum Design Helps Spiking Neural Networks to Classify Time Series

Chenxi Sun [1 2 3] **Hongyan Li** [1 2 3] **Moxian Song** [1 2 3] **Derun Cai** [1 2 3] **Shenda Hong** [4 5]

Abstract

Spiking Neural Networks (SNNs) have a greater potential for modeling time series data than Artificial Neural Networks (ANNs), due to their inherent neuron dynamics and low energy consumption. However, it is difficult to demonstrate their superiority in classification accuracy, because current efforts mainly focus on designing better network structures. In this work, enlighten by brain-inspired science, we find that, not only the structure but also the learning process should be human-like. To achieve this, we investigate the power of Curriculum Learning (CL) on SNNs by designing a novel method named `CSNN` with two theoretically guaranteed mechanisms: The active-to-dormant training order makes the curriculum similar to that of human learning and suitable for spiking neurons; The value-based regional encoding makes the neuron activity to mimic the brain memory when learning sequential data. Experiments on multiple time series sources including simulated, sensor, motion, and healthcare demonstrate that CL has a more positive effect on SNNs than ANNs with about twice the accuracy change, and `CSNN` can increase about 3% SNNs' accuracy by improving network sparsity, neuron firing status, anti-noise ability, and convergence speed.

1. Introduction

Despite producing positive results in the classification of time series, Artificial Neural Networks (ANNs) appear to reach the bottleneck stage: Time series exhibits dynamic evolution, whereas most ANNs are static. Although the purpose is to create brain-like dynamics, ANNs only adhere to the connection mode and do not penetrate deeply into the neurons. To model more data dynamics, even Recurrent Neural Networks (RNNs), which are inherently dynamic, need additional mechanisms (Sun et al., 2021). Meanwhile, accuracy and lightness are frequently incompatible with ANNs, while ambient-assisted living represents the general trend and favors high-efficient and low-consumed models.

A growing efficient paradigm is Spiking Neural Networks (SNNs). They mimic the brain capacity, specifically the intricate dynamics of spiking neurons and the plastic synapses bridging them, and are scientifically plausible. Since each neuron is a dynamic system that can learn both the time and the order relation, it is more suited to depict evolution in real-world time series. Meanwhile, by processing the data as sparse spike events, SNNs offer low power usage.

However, SNNs have struggled to demonstrate a clear advantage over ANNs in accuracy due to the information loss during spike coding, the incomplete modeling of neurotransmitter transmission, and the inability of gradient backpropagation (Yin et al., 2021). Consequently, the majority of the effort to increase the accuracy begins with these model structure-related factors. But back to the original intention, SNNs are more brain-like, not only the model structure but also the learning process should resemble that of humans. People usually learn easier knowledge before more complicated ones. Curriculum Learning (CL) has shown that an easy-to-hard training order can enhance the model performance and generalization power for ANNs (Hacohen & Weinshall, 2019). For SNNs, however, this study is lacking.

The capacity of CL to SNN in classifying time series is still unknown to us: ANNs' curriculum may not adapt to SNNs due to their structural differences; Theoretical principles are required to lead SNNs' curriculum; The designed curriculum should be adjusted to account for spiking features; The classification will be impacted by the way to acquire each time series in addition to the learning order among them (Sun et al., 2022). Different areas of the brain assist the memory for different pieces in a sequence (Xie et al., 2022). However, by default, all of the neurons in an SNN that process various subparts of a time series are the same.

This work studies the power of CL in training SNNs for the first time. We recognize the temporal dynamics of Recurrent SNN (RSNN) are advantageous for modeling and classify-

ing time series. Based on experimental observations about how training orders and memory modes affect SNNs via spiking trains and neuron firing, and through theoretically guaranteed insights, objectives, and procedures, we propose a Curriculum for SNN (CSNN) with two mechanisms:

- Active-to-dormant training order mechanism (A2D) uses the sample's activity to customize the training order. The output neuron firing frequency that corresponds to the sample's class label serves as a gauge of its activity.
- Value-based regional encoding mechanism (RE) uses various spiking neuron clusters to encode input spikes that are differentiated by observed values, imitating the regional pattern in the brain when memorizing sequential data.

We show their rationality and effectiveness through theoretical analysis and experiments on three real-world datasets.

2. Related Work

2.1. Classification of Time Series (CTS)

Time Series (TS) data is present in practically every task that calls for some kind of human cognitive process due to their inherent temporal ordering (Fawaz et al., 2019). A TS dataset $\mathcal{D} = \{(X_i, C_i)\}_{i=1}^N$ has N samples. A sample $X_i = \{x_t\}_{t=1}^T$ has T observed values and time and is labeled with a class $C_i \in \mathcal{C}$. The CTS task is $f : X \to C$ with model f. Many ANNs have achieved SOTA for CTS tasks, which can be summarized into three categories: recurrent networks like LSTM (Zhao et al., 2020), convolutional networks like 1D-CNN (Jiang et al., 2021), and attention networks like Transformer (Zerveas et al., 2021). But the dynamics of real-world TS actually vary, such as multiple scales, uneven time intervals, and irregular sampling (Sun et al., 2020a). Current solutions often design additional mechanisms for ANNs artificiality rather than revise them internally.

2.2. Spiking Neural Networks (SNNs)

An SNN consists of neurons that propagate information from a pressynapse to a postsynapse. At the time t, as the synaptic current reaches the neuron it will alter its membrane potential $v(t)$ by a certain amount. If $v(t)$ reaches a threshold V_{th}, the pressynapse will emit a spike and reset $v(t)$ to V_0. In an SNN, each neuron has its own dynamics over time. This expands the modeling options for TS. Most current work for this biologically plausible model examines the network structure, such as the Leaky Integrate and Fire (LIF) model (Gütig & Sompolinsky, 2006) and the gradient surrogate updating strategy (Kheradpisheh & Masquelier, 2020). For modeling TS, SNN (Fang et al., 2020), RSNN (Yin et al., 2021), and LSNN (Bellec et al., 2018) are proposed, but their accuracy is still behind that of non-spiking ANNs of approximate architecture (Zhang et al., 2021).

2.3. Curriculum Learning (CL)

CL is motivated by the curriculum in human learning, attempts at imposing some structure on the training set. It gives a sequence of input mini-batches $\mathcal{D} \to \mathbb{B} = [\mathcal{B}_b]_{b=1}^B$. Two subtasks are scoring f_s and pacing f_p: f_s ranks samples, $f_s : \mathcal{D} \to \mathbb{R} = [(X_i, C_i)]_{i=1}^N$, if $f_s(i) < f_s(j), (X_i, C_i) \succ (X_j, C_j)$, such as knowledge transfer and self-taught strategies (Castells et al., 2020); f_p determines which sample is presented to the network by giving a sequence of subsets $\mathbb{B}$ of size $f_p(b) = |\mathcal{B}_b|$, such as single-step and exponential functions (Lin et al., 2022). Most work shows that the easy-to-hard training order outperforms the random shuffling (Hacohen & Weinshall, 2019). For CTS tasks, a few methods such as confidence-based CL are proposed (Sun et al., 2022). But the examination of curriculum tailored to TS' characteristics is not extensive. Most importantly, none of them can guarantee that they would have a positive effect on SNNs because they are all ANN-specific. Research on CL for SNNs is anticipated.

3. Methods

As shown in Figure 1, the proposed curriculum consists of two mechanisms[1]: The active-to-dormant training order mechanism (A2D) is in Section 3.1; The value-based regional encoding mechanism (RE) is in Section 3.2. Each of them is introduced through a theoretically supported process that includes INSIGHT, OBJECTIVE, and PROCEDURE.

3.1. Active-to-dormant Training Order (A2D)

INSIGHT: DIFFERENT TRAINING ORDERS MAKE THE SPIKING NEURON OUTPUT DIFFERENT SPIKE TRAINS

We adopt the a widely used LIF neuron. Each input spike induces a charge in the neuron's membrane potential, called a Post Synaptic Potential (PSP). In Equation 1, t_i is the arrival time of i-th input spike s_i. $K(t)$ is the synapse kernel, where τ_m and τ_s are time constants. $V_0 = \frac{\eta}{\eta-1}$ and $\eta = \frac{\tau_m}{\tau_s}$ scale the maximum value of $K(t)$ to 1.

$$\text{PSP}(t) = \sum_{t_i}^{t_i < t} K(t - t_i)s_i, \ K(t) = V_0(e^{-\frac{t}{\tau_m}} - e^{-\frac{t}{\tau_s}}) \quad (1)$$

The neuron accumulates all input PSPs and then forms the membrane potential $v(t)$. In Equation 2, N_I is the number of input synapse. w_i is the weight associated with each input synapse. $t_s < t$ is the time when the neuron generates an output spike. And the membrane potential is decreased by a factor of the threshold voltage V_{th}. This serves as the

---

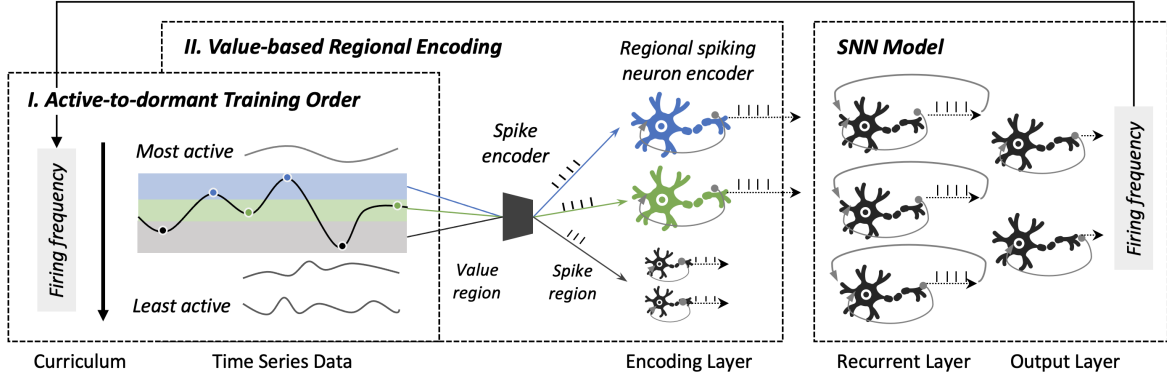[1]All theorems, propositions and proofs involved in the proposed method will be thoroughly discussed in Appendix A.

Figure 1. Curriculum of Time Series Data for Recurrent Spiking Neural Network

reset mechanism at the time of spike.

$$v(t) = \sum_{i}^{N_I} w_i \mathrm{PSP}_i(t) - V_{th} \sum_{t_s}^{t_s < t} e^{-\frac{t-t_s}{\tau}} \quad (2)$$

We define the input spike train $I[t]$ and the output spike train $O[t]$ as sequences of time shifted Dirac delta function, where $s[t] = 1$ denotes a spike received at time t, otherwise $s_i = 0$. $y[t] > 0$ satisfies $v(t) > V_{th}$, otherwise $y[t] = 0$

$$I[t] = \sum_{i}^{t} s[n]\delta(t-i), \quad O[t] = \sum_{i}^{t} y[n]\delta(t-i) \quad (3)$$

Theorem 1. *In SNN, different input orders of spike trains make the neuron output different spike trains.*

Proof. Most simply, assuming an SNN with parameters w initialized randomly under a Gaussian distribution $\mathcal{N}(\mu, \sigma^2)$, $\frac{\mu}{2} < V_{th} < \mu$, an l-length input sequence with all-one spike $S_0 = (1)^l$, and an l-length input sequence with half-one spike $S_1 = (0)^{\frac{l}{2}} \wedge (1)^{\frac{l}{2}}$, when giving two training order $S_0 \rightarrow S_1$ and $S_1 \rightarrow S_0$ to SNN, the membrane potential v of one neuron in the first layer may output two different spike trains $O_0 = (1, 1) \neq O_1 = (0, 1)$. $\square$

The importance of the training order is demonstrated by Theorem 1. And different output spike trains will result in different update times and degrees of parameters, finally forming different SNN (Chen et al., 2022). Meanwhile, through the proof, the training order also affects whether a sample participates in updating parameters of SNN. For example, in $S_1 \rightarrow S_0$, S_1 does not make the neuron fire so that the SNN is not updated. Thus, the training order may also affect training stability, efficiency, and noise resistance.

OBJECTIVE: CL REQUIRES CONSISTENCY BETWEEN OBJECTIVE FUNCTION AND SAMPLING PROBABILITY

We define a maximum function $U_\vartheta(X_i)$ as the objective of CTS task. The hyper-parameter set ϑ represents a model and

its different settings will produce different model functions.

$$\mathcal{U}(\vartheta) = \hat{\mathbb{E}}[U_\vartheta] = \sum_{i=1}^{N} U_\vartheta(X_i), \ \tilde{\vartheta} = \arg\max_\vartheta \mathcal{U}(\vartheta) \quad (4)$$

CL provides a Bayesian prior for data sampling $p_i = p(X_i)$. For example, a non-increasing function of the difficulty level of X_i, $p(X_i) = \frac{1}{N}$ for N training samples whose difficulty score $< \epsilon$, and $p(X_i) = 0$ otherwise. The threshold ϵ is determined by the pacing function which drives a monotonic increase in the number B.

$$\mathcal{U}_p(\vartheta) = \hat{\mathbb{E}}_p[U_\vartheta] = \sum_{i=1}^{N} U_\vartheta(X_i)p(X_i) \quad (5)$$

Theorem 2. *The difference between objectives $\mathcal{U}_p$ and $\mathcal{U}$, which are computed with and without curriculum prior p, is the covariance between U_ϑ and p.*

$$\mathcal{U}_p(\vartheta) = \mathcal{U}(\vartheta) + \hat{\mathrm{Cov}}[U_\vartheta, p] \quad (6)$$

Proof. Equation 6 is obtained from Equation 5: $\mathcal{U}_p(\vartheta) = \sum_{i=1}^{N} U_\vartheta(X_i)p(X_i) = \sum_{i=1}^{N} U_\vartheta(X_i)p(X_i) - 2N\hat{\mathbb{E}}(U_\vartheta)\hat{\mathbb{E}}(p) + 2N\hat{\mathbb{E}}(U_\vartheta)\hat{\mathbb{E}}(p) = \sum_{i=1}^{N}(U_\vartheta(X_i) - \hat{\mathbb{E}}[U_\vartheta])(p_i - \hat{\mathbb{E}}[p]) + N\hat{\mathbb{E}}(U_\vartheta)\hat{\mathbb{E}}(p) = \hat{\mathrm{Cov}}[U_\vartheta, p] + \mathcal{U}(\vartheta)$ $\square$

Theorem 3. *In CL, the optimal $\tilde{\vartheta}$ maximizes the covariance between p and U_ϑ: $\tilde{\vartheta} = \arg\max_\vartheta \mathcal{U}(\vartheta) = \arg\max_\vartheta \hat{\mathrm{Cov}}[U_\vartheta, p]$, satisfying:*

$$\tilde{\vartheta} = \arg\max_\vartheta \mathcal{U}(\vartheta) = \arg\max_\vartheta \mathcal{U}_p(\vartheta)$$
$$\forall \vartheta \quad \mathcal{U}_p(\tilde{\vartheta}) - \mathcal{U}_p(\vartheta) \geq \mathcal{U}(\tilde{\vartheta}) - \mathcal{U}(\vartheta) \quad (7)$$

Proof. From Theorem 2, $\mathcal{U}_p(\tilde{\vartheta}) - \mathcal{U}_p(\vartheta) = \mathcal{U}_p(\tilde{\vartheta}) - \mathcal{U}(\vartheta) - \hat{\mathrm{Cov}}[U_\vartheta, p] \geq \mathcal{U}_p(\tilde{\vartheta}) - \mathcal{U}(\vartheta) - \hat{\mathrm{Cov}}[U_{\tilde{\vartheta}}, p] = \mathcal{U}(\tilde{\vartheta}) - \mathcal{U}(\vartheta)$ $\square$

It demonstrates that, more so than with any other $U_\vartheta(X)$, p has a positive correlation with the optimal $U_{\tilde{\vartheta}}(X)$. The gradients in the new optimization landscape may thus be

generally steeper in the direction of the optimal parameter $\tilde{\vartheta}$. The original problem's global optimum is present in the updated optimization landscape created by CL, sharing the trait of having a more apparent global maximum.

PROCEDURE: THE ACTIVE-TO-DORMANT TRAINING ORDER FOR SNNs MEETS THE GOAL OF CL

What sort of training order can accommodate SNN while achieving the CL's goal? We demonstrate that the proposed active-to-dormant training order satisfies Theorem 2, 3.

We measure the activity pC_i of a TS sample X_i based on the distribution of firing frequency in the output layer in Equation 8. L is the number of network layers, $O_i^L[t]$ denotes the output of last layer, N_C is the neuron number of last layer. Thus, an ideal curriculum is the prior corresponding to the optimal hypothesis $p_i = \frac{e^{pC(X_i)}}{P}, P = \sum_{i=1}^{N} e^{pC(X_i)}$.

$$pC(X_i) = \frac{e^{\sum_t^T O_i^L[t]}}{\sum_{j=1}^{N_c} e^{\sum_t^T O_j^L[t]}} \quad (8)$$

In fact, Equation 8 is consistent with the objective of the CTS task. In SNN, the neuron in the output layer that fires most frequently represents the result. Thus, pC_i and N_C can be seen as the calculated probability of each class and the class number. The cross-entropy loss is defined as Equation 9, where C_i is the class label. $L_\vartheta(X_i)$ denotes the loss of hypothesis defined by ϑ when given an sample X_i. The empirical risk minimization compute the best hypothesis of $\tilde{\vartheta}$ from the training data.

$$\mathcal{L} = \hat{\mathbb{E}}[L], \; L(X_i) = -C_i \log(pC_i) \quad (9)$$

$$\tilde{\vartheta} = \arg\min_\vartheta \mathcal{L}(\vartheta) = \arg\min_\vartheta \sum_{i=1}^{N} L_\vartheta(X_i)$$
$$= \arg\max_\vartheta \exp\left(-\sum_{i=1}^{N} L_\vartheta(X_i)\right) = \arg\max_\vartheta \prod_{i=1}^{N} e^{-L_\vartheta(X_i)}$$

According to Equation 9, we specify U and p based on the maximum likelihood estimation with probability for empirical risk minimization $P(\vartheta|X) \propto e^{-L_\vartheta(X)}$.

$$U_\vartheta(X_i) = e^{-L_\vartheta(X_i)} \quad (10)$$

$$p_i = \frac{e^{-L_{\tilde{\vartheta}}(X_i)}}{\sum_i^N e^{-L_{\tilde{\vartheta}}(X_i)}} = \frac{U_{\tilde{\vartheta}}(X_i)}{P} \quad (11)$$

Proposition 1. *When using the active-to-dormant training order, Theorem 3 holds if the variance of the maximum function is roughly constant in the relevant range of plausible parameter values.*

$$\mathcal{U}_p(\tilde{\vartheta}) - \mathcal{U}_p(\vartheta) \geq \mathcal{U}(\tilde{\vartheta}) - \mathcal{U}(\vartheta) \quad \forall \vartheta : \text{Cov}[U_\vartheta, U_{\tilde{\vartheta}}] \leq \text{Var}[U_{\tilde{\vartheta}}]$$

Proof. From Equation 11, $\mathcal{U}_p(\vartheta) = \mathcal{U}(\vartheta) + \frac{1}{P}\text{Cov}[U_\vartheta, U_{\tilde{\vartheta}}]$. Then, at the optimal point $\tilde{\vartheta}$: $\mathcal{U}_p(\tilde{\vartheta}) = \mathcal{U}(\tilde{\vartheta}) + \frac{1}{P}\text{Var}[U_{\tilde{\vartheta}}]$; at any other point: $\mathcal{U}_p(\vartheta) \leq \mathcal{U}(\tilde{\vartheta}) + \frac{1}{P}\sqrt{\text{Var}[U_\vartheta]\text{Var}[U_{\tilde{\vartheta}}]}$. Assuming a constant $b = \text{Var}[U_\vartheta]$, Theorem 3 follows $\mathcal{U}_p(\vartheta) \leq \mathcal{U}(\tilde{\vartheta}) + \frac{b}{P} = \mathcal{U}_p(\tilde{\vartheta})$, i.e. $\tilde{\vartheta} = \arg\max_\vartheta \mathcal{U}_p(\vartheta)$. $\quad \square$

According to Proposition 1, the optimization landscape is altered in order to emphasize the contrast between the vector of optimal parameters and all other parameter values that are covariant with the optimal solution. And our CL strategy $\tilde{\vartheta}$, active-to-dormant training order, can make the variance of sample activity $\text{Var}[U_{\tilde{\vartheta}}]$ greater. From the perspective of the loss function, the strategy of active-to-dormant training order for SNNs is consistent with that of easy-to-hard training order for ANNs in the classical CL.

3.2. Value-based Regional Encoding (RE)

INSIGHT: SEQUENTIAL DATA ARE MEMORIZED BY THE HUMAN BRAIN THROUGH DISTINCT REGIONS

According to recent studies (Xie et al., 2022), the brain memorizes sequential information in multiple regions with a geometrical structure rather than just one. This type of regional memory can boost spike firing. Inspired by this insight, we suggest a regional spiking mechanism based on TS values for SNN. In this way, on the basis of imitating the information transmission mechanism of the brain, SNN also mimics the sequence processing mechanism of the brain.

OBJECTIVE: CL BENEFITS FROM SNN'S IMPROVED SAMPLE DISCRIMINATION.

Based on Proposition 1, making $\text{Var}[U_{\tilde{\vartheta}}] - \text{Cov}[U_\vartheta, U_{\tilde{\vartheta}}]$ larger will boost the advantages of utilizing CL for SNN on the CTS task. To achieve this goal, $\text{Var}[U_{\tilde{\vartheta}}]$ should be larger, and/or $\text{Cov}[U_\vartheta, U_{\tilde{\vartheta}}]$ should be smaller, i.e., the variance of each sample's $U_{\tilde{\vartheta}}(X_i)$ becomes larger, or/and $U_{\tilde{\vartheta}}(X)$ diverges from $U_\vartheta(X)$ more.

Theorem 4. *The difference between the objective score with CL and that without CL will be greater if there is a larger score discrepancy between each sample.*

Proof. Without CL, since the training samples are fixed, $\text{Var}[U_\vartheta]$ is constant; With CL, based on Equation 11, as $P \approx \mathbb{E}[e^{-L(X_i)}]$ is constant, $\text{Var}[U_{\tilde{\vartheta}}] \propto \text{Var}[p]$. Thus, $\text{Var}[p] \uparrow \rightarrow \text{Var}[U_{\tilde{\vartheta}}] \uparrow \rightarrow \text{Cov}[U_\vartheta, U_{\tilde{\vartheta}}] \downarrow \quad \square$

Theorem 4 states that if the CL strategy increases the difference among the score value p of each sample, $\text{Var}[U_{\tilde{\vartheta}}] - \text{Cov}[U_\vartheta, U_{\tilde{\vartheta}}]$ will be larger, CL's benefits will be more clear.

PROCEDURE: THE VALUE-BASED REGIONAL ENCODING BOOSTS SNN'S DIFFERENTIAL RESPONSE TO SAMPLES

How to make SNN response to various TS samples differ more? We suggest the value-based regional encoding mechanism by replicating human brain processing sequence.

For a TS $X = \{x_t\}_{t=1}^T$, in the classical SNNs, the input spike train $I[t]$ in Equation 3 corresponding to each observed value x_t will be input to all N_{input} neurons of the input layer, so all membrane potentials are Equation 2 with $t = 1, ..., T$.

Different from the input of classical SNNs, in value-based regional encoding mechanism, different neurons receive the input having different observed value: We divide the interval $[\min(x), \max(x)]$ into M subintervals $\mathbb{I} = \{\mathcal{I}_m\}_{m=1}^M, M \leq N_{\text{input}}$, thus every $\frac{N_{\text{input}}}{M}$ neurons are responsible for a numerical interval and receive different input spike trains. The membrane potential of neurons having $\mathcal{I}_m$ are Equation 2 with t satisfing $x_t \in \mathcal{I}_m$.

Proposition 2. *The regional encoding contributes to SNNs' CL by increasing the variation of sample activity and assisting the model's quick response to input changes.*

Proof. At time t, we call spiking neurons with $x_t \in \mathcal{I}_m$ as excitatory neurons S_E and neurons with $x_t \notin \mathcal{I}_m$ as inhibitory neurons S_I. For S_I, the membrane potential is only discharged but not charged, i.e. Equation 2 only has the rightmost item. Thus, we can regard it as an extreme case of feed-forward and feed-back inhibition. The inhibition changes piking rate (Dz et al., 2022), the value of Equation 10 increases under the true class label so that the difference among computed values of Equation 4 of samples with different labels becomes larger. Thus, $\text{Var}[U_{\tilde{y}}]$ increases.

The neuronal input is given by external and recurrent input $I_i[t] = I_i^{ext}[t] + I_i^{rec}[t]$. The external inputs have excitatory (e) $K_E = P_C S_E$ and inhibitory (i) $K_I = P_C S_I$ with a probability P_C. The recurrent inputs are Poisson spike trains $I_i^{rec}[t] = \mu_i^{rec} + \sigma_i^{rec}\xi_i^{rec}$ (Torab & Kamen, 2001). $\mu_{e/i} = \mu_{rec,e/i} + f_{e/i}\mu_{ext}, \sigma_{e/i}^2 = \sigma_{ext}^2 + \sigma_{rec,e/i}^2, \beta_{e/i} = \frac{\sigma_{e/i}^2}{\mu_{e/i}}$ are inputs' mean, variance, variance-to-mean radio. σ_{ext}^2 is usually very small and $\beta_{e/i}$ is a constant irrespective to external inputs. The neural firing rate is $r_{e/i} = \frac{\mu_{e/i}}{V_{th}V_0} \propto \mu_{ext}$. It linearly encodes the external input mean, ensuring the network's response to input changes very fast. $\square$

3.3. Curriculum for SNNs (CSNN)

CLASSIFICATION MODEL. Direct implementation of the SNN model defined by Equation 2 is not practical. We use an incremental way to update the PSP as indicated in Equation 12. It can be derived from the spike response model in discrete time domain. Each neuron has a recurrent mode. l, i, j are layer, neuron, input index. N_l denotes the

---

Algorithm 1 CSNN
  // A2D MECHANISM
1: Get sores $\mathcal{P} \leftarrow$ Equation 13
2: Get the sorted TS dataset $\mathbb{R}$ by $\mathcal{P}$
3: Initialize mini-batches $\mathbb{B} \leftarrow [\ ]$
4: **for** $b = 1$ to B **do**
5:     Get size $|\mathcal{B}_b| \leftarrow$ Equation 14
6:     Get mini-batch $\mathcal{B}_b \leftarrow \mathbb{R}[(X_i, C_i)]_{i=1}^{|\mathcal{B}_b|}$
7:     $\mathbb{B} \leftarrow \mathcal{B}_b$
8: **end for**
  // RE MECHANISM
9: Construct f_e with M encoder clusters
10: **for** $b = 1$ to B **do**
11:     Get spiking trains $\mathbb{I} \leftarrow f_e(\mathcal{B}_b)$
12:     Train RSNN with $\mathbb{I}$
13: **end for**

---

number of neurons in l-th layer. $I[t], R[t], O[t]$ are input current, reset voltage, neuron output. $H(x)$ is a Heaviside step function: $H(x) = 0,$ if $x < 0,$ otherwise 1.

$$
\begin{aligned}
V_i^l[t] &= I_i^l[t] - V_{th}R_i^l[t], \quad I_i^l[t] = V_0 \sum_j^{M_{l-1}} w_{i,j}^l(M_i^l[t] - H_i^l[t]) \\
M_i^l[t] &= \alpha N_i^l[t-1] + O_j^{l-1}[t], \quad H_i^l[t] = \beta H_i^l[t-1] + O_j^{l-1}[t] \\
R_i^l[t] &= \gamma R_i^l[t] + O_i^l[t-1], \quad O_i^l[t] = H(V_i^l[t] - V_{th})
\end{aligned}
\tag{12}
$$

To encode TS into spike sequences, we utilize a population of current-based integrate and fire neurons as encoder and pre-train the encoder using a neural engineering framework (Fang et al., 2020); To train SNN, we employ Equation 9 as the loss function and update SNN's parameters by employing the back-propagation through time and the gradient surrogate method (sigmoid) during training process (Kheradpisheh & Masquelier, 2020).

CURRICULUM DESIGN. Algorithm 1 displays the proposed approach (CSNN = A2D + RE). For A2D, the scoring function is based on Equation 11, the pacing function is the exponential pacing in Equation 14; For RE, there are N_{input} spiking neuron receivers and M TS value intervals, every $\frac{N_{\text{input}}}{M}$ neurons belong to a cluster $M < N_{\text{input}}$.

$$
f_s(X_i) = p_i = \frac{e^{-L(X_i)}}{\sum_i^N e^{-L(X_i)}}
\tag{13}
$$

$$
f_p(m) = \min(\text{start\_percent}\cdot(1+\lfloor\frac{m}{\text{step\_length}}\rfloor), 1)\cdot N
\tag{14}
$$

4. Experiments

4.1. Experimental Setup

DATASETS. The benchmark UCR archive (Dau et al., 2019) has univariate and regularly-sampled TS data, consisting of

	$\tau_m(\mu,\sigma)$	$\tau_s(\mu,\sigma)$	$\tau(\mu,\sigma)$	a	bias	sp	ss	η	η decay(type)	M	$\frac{N_{\text{input}}}{M}$
UCR	(20,5)	(150,10)	(20,5)	20	0(fixed)	5%	50	1e-2	.5per10(step)	[5,10]	16
SEPSIS	(20,5)	(150,50)	(20,5)	20	0(fixed)	10%	2,000	1e-2	.5per20(step)	5	32
COVID-19	(20,5)	(150,50)	(20,5)	20	0(fixed)	5%	350	1e-2	.5per20(step)	5	16

Table 1. Hyper-parameter Setting of CSNN

	# Classes	RNN	LSTM	1D-CNN	Transformer	SNN	RSNN	LSNN	CSNN
Coffee	2	.998±.001(4)	1.00±.002(**1**)	1.00±.002(**1**)	.998±.001(4)	.986±.002(6)	.986±.001(6)	.986±.004(6)	1.00±.002(**1**)
GunPoint	2	.987±.001(5)	1.00±.003(**1**)	1.00±.000(**1**)	1.00±.003(**1**)	.986±.004(7)	.987±.002(5)	.986±.003(7)	1.00±.003(**1**)
MoteStrain	2	.892±.008(3)	.895±.010(**1**)	.890±.010(5)	.891±.014(4)	.865±.015(7)	.869±.014(6)	.865±.016(7)	.894±.011(2)
Computers	2	.844±.010(4)	.849±.011(2)	.851±.009(**1**)	.843±.012(5)	.803±.010(8)	.809±.012(6)	.806±.012(7)	.849±.006(2)
Wafer	2	.999±.000(3)	.999±.000(3)	.999±.000(3)	1.00±.000(**1**)	.977±.001(6)	.977±.001(6)	.977±.001(6)	1.00±.000(**1**)
Lightning	2	.831±.006(3)	.833±.006(2)	.830±.007(5)	.834±.008(**1**)	.806±.013(8)	.815±.010(7)	.816±.014(6)	.831±.006(3)
Yoga	2	.875±.012(6)	.886±.011(3)	.886±.013(3)	.886±.011(3)	.875±.012(6)	.875±.016(6)	.888±.014(2)	.901±.010(**1**)
CBF	3	1.00±.000(**1**)	1.00±.000(**1**)	1.00±.000(**1**)	.998±.000(6)	.996±.002(6)	.996±.002(6)	.996±.003(6)	1.00±.009(**1**)
BME	3	.997±.001(4)	.977±.001(4)	1.00±.000(**1**)	.999±.001(3)	.976±.002(7)	.977±.001(4)	.976±.002(7)	1.00±.009(**1**)
Trace	4	1.00±.000(**1**)	1.00±.000(**1**)	.999±.001(5)	1.00±.000(**1**)	.999±.001(5)	.999±.001(5)	.999±.001(5)	1.00±.000(**1**)
Oliveoil	4	.899±.011(6)	.923±.009(3)	.923±.008(3)	.931±.012(**1**)	.868±.013(8)	.879±.013(7)	.906±.010(5)	.924±.008(2)
Beef	5	.835±.012(5)	.844±.013(4)	.848±.011(2)	.845±.011(3)	.805±.015(8)	.810±.012(6)	.808±.014(7)	.849±.011(**1**)
Worms	5	.709±.011(6)	.709±.012(6)	.723±.015(2)	.723±.010(2)	.709±.014(6)	.710±.018(5)	.711±.012(4)	.724±.015(**1**)
Symbols	6	.954±.005(5)	.962±.006(2)	.963±.004(**1**)	.957±.002(4)	.905±.009(8)	.915±.009(6)	.912±.007(7)	.961±.003(3)
Synthetic	6	1.00±.000(**1**)	1.00±.000(**1**)	1.00±.000(**1**)	.998±.001(5)	.996±.001(6)	.996±.002(6)	.996±.001(6)	1.00±.009(**1**)
Rank		3.6	2.3	2.3	2.7	6.8	5.7	6.2	**1.5**
SEPSIS	2	.853±.015(7)	.855±.013(4)	.858±.015(2)	.854±.011(6)	.829±.012(8)	.856±.009(3)	.855±.013(4)	**.870±.010(1)**
COVID-19	2	.963±.013(6)	.968±.013(2)	.954±.013(5)	.941±.012(8)	.942±.010(7)	.955±.009(3)	.955±.011(3)	**.969±.008(1)**

Table 2. Classification Accuracy ↑ and Performance Ranking ↓ of Methods

128 TS datasets. We select 15 datasets covering multiple data types (spectro, sensor, simulated, motion) and classification tasks (binary-, three-, four-, five-, six-classification). Both two real-world healthcare datasets have multivariate and irregularly-sampled TS data: SEPSIS dataset (Reyna et al., 2019) has 30,336 records with 2,359 diagnosed sepsis. Each TS sample has 40 related patient features. Early diagnosis is critical to improving sepsis outcome (Seymour et al., 2017); COVID-19 dataset (Yan et al., 2020) has 6,877 blood samples of 485 COVID-19 patients from Tongji Hospital, Wuhan, China. Each sample has 74 laboratory test features. Mortality prediction helps for timely treatment and allocation of medical resources (Sun et al., 2020b).

BASELINES. The SOTA ANNs include RNN, LSTM (Zhao et al., 2020), 1D-CNN (Jiang et al., 2021), and Transformer (Zerveas et al., 2021). The SOTA SNNs include SNN (Fang et al., 2020), RSNN (Yin et al., 2021), and LSNN (Bellec et al., 2018). SNNs (SNN, RSNN, LSNN) are the spiking neuron versions of the classical ANNs (MLP, SNN, LSTM). The basic CTS model in CSNN is RSNN.

HYPER-PARAMETERS. SNNs need the initialization of both the weight and the hyper-parameters of the spiking neurons (time constants, thresholds, starting potential). We initialize the starting value of the membrane potential $V_i^l[0]$ is initialized with a random value distributed uniformly in the range $[0, a + 1.8\eta]$, η is the learning rate; We randomly initialize the time constants τ_m, τ_s, τ following a tight normal distribution μ, σ with constant, uniform, and normal initializers; We test the pacing parameters in range $[2\%, 20\%]$ for start percent sp and range $[50, 2500]$ for step size ss; We test the internal number of RE in range $[5, 10]$ and the neuron number of a cluster in $\{8, 16, 32, 64\}$. Table 1 lists the final hyper-parameter setting. This setting also confirms that the assumptions $\frac{\mu}{2} < V_{th} < \mu$ we made in proving Theorem 1 often exist in practice. Figure 3(c) shows that the normal initializer achieves the best performance. A2D, RE, and the typical initializer make SNNs more active and less sparse during the initial training stage, allowing converging faster.

4.2. Classification Accuracy

CSNN significantly improves the accuracy of SNNs for CTS task and makes SNNs (SNN, RSNN, LSNN) achieve performance comparable to deep ANNs (RNN, LSTM, 1D-CNN, Transformer). The 5-fold cross-validation method yields results that are presented as mean ± standard deviation. The classification accuracy is evaluated by Area Under Curve of Receiver Operating Characteristic (AUC-ROC, the higher the better) and its Confidence Interval (AUC-CI).

CSNN has the highest classification accuracy on most datasets among all tested methods as shown in Table 2. It has a significant improvement in the average accuracy according to the Bonferroni-Dunn test with $\alpha = 0.05$, $2.949\sqrt{\frac{7\times(7+1)}{6\times5\times3}} = 2.62$ (critical difference) < 4.74 (average rank of baselines). CSNN can produce stable results as
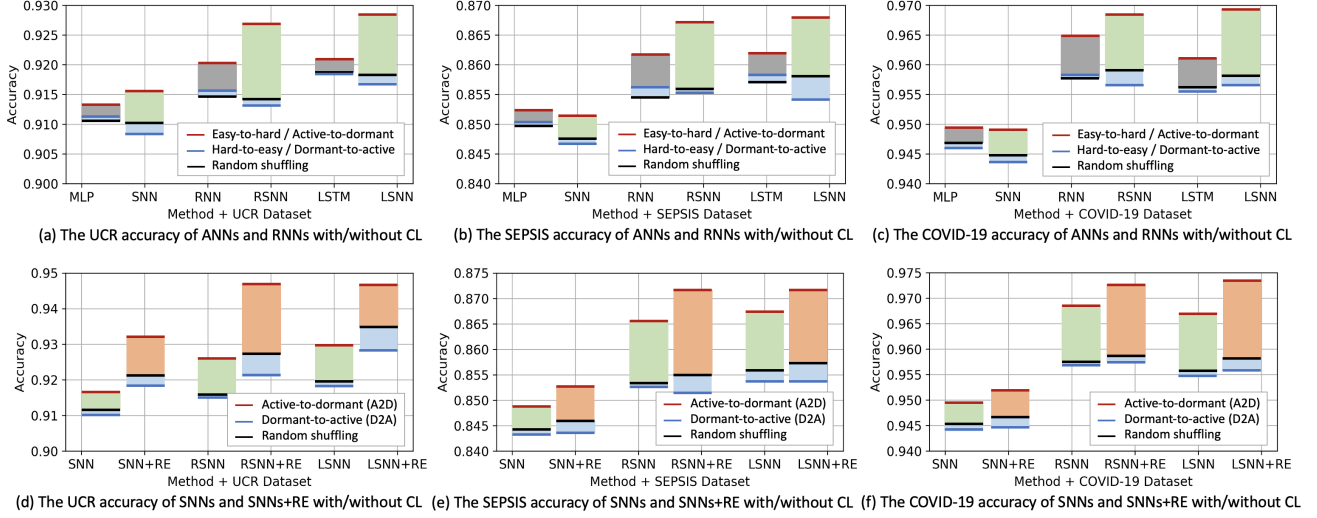
Figure 2. Changes in Classification Accuracy of Different ANNs and SNNs after Applying Curriculum Learning

the 5-fold cross-validation results are all within the AUC-CI. For example, the accuracy of COVID-19 mortality classification (0.971 ± 0.008) is in the AUC-CI (0.971 ± 0.012).

SNNs are more suitable for modeling irregularly-sampled TS than ANNs. SNNs perform better than ANNs on SEPSIS and COVID-19 datasets. ANNs ignore the effect of uneven time intervals on value dependence, whereas SNNs have a decay mechanism over time for this issue: In inference, the model can be simulated in an event-driven manner, i.e. computation is only required when a spike event occurs. Thus, TS data is not required to have a uniform time interval as SNNs calculate based on time records. Suppose at t, $M[t]$ is known. In Equation 15, after Δt unit time later, i.e. at time $t' = t + \Delta t$, $M[t]$ decays over time without input spike; $M[t]$ has an instantaneous unit charge with an input spike. And the similar update rule can also apply for states $H[t]$ and $R[t]$ with $H[t'] = H[t]e^{\frac{-\Delta t}{\tau_s}}$, $R[t'] = H[t]e^{\frac{-\Delta t}{\tau}}$.

$$\text{No input spike}: M[t'] = \sum_{t_i < t}^{t_i} e^{-\frac{t + \Delta t - t_i}{\tau_m}} = M[t]e^{\frac{-\Delta t}{\tau_m}} \quad (15)$$

$$\text{An input spike}: M[t'] = M[t]e^{\frac{-\Delta t}{\tau_m}} + 1$$

4.3. Curriculum Learning Performance

THE POWER OF ACTIVE-TO-DORMANT TRAINING ORDER MECHANISM (A2D)

The orderly training has a greater impact on SNNs than ANNs with about twice the accuracy change. And CSNN can improve the classification accuracy, network sparsity, firing status, and anti-noise ability of SNNs. In this experiment, we apply our A2D to SNNs and the easy-to-hard training order (E2H) (Hacohen & Weinshall, 2019) to ANNs. The dormant-to-active training order (D2A) and the hard-to-easy

training order (H2E) are their anti-curriculum.

The CTS accuracy of SNNs using A2D is improved more than that of ANNs using E2H (The green rectangle is bigger than the gray rectangle) as shown in Figure 2(a)-(c). Meanwhile, the anti-curriculum will negatively affect SNNs (The blue line is below the black line), but sometimes positively affect ANNs (The blue line is above the black line). This demonstrates that SNNs are more impacted by CL than ANNs are (The distance between the red line and the blue line of SNNs is farther than that of ANNs).

SNNs communicate sparingly. A2D can adjust the firing status and network sparsity of the trained SNNs when classify TS data as shown in Figure 3(a). The sparsity ratio represents the proportion of neurons that have not been fired in total spiking neurons. After using A2D, both the CTS accuracy and the sparsity ratio are increased, where RSNN's sparsity changes the most among the tested SNNs. And the sparsity of SNNs with wider structure is more affected than that of SNNs with wider structure as shown in Figure 3(c). This finding opens up more opportunities for using optimization techniques like pruning and quantization, emphasizing the benefits of being lightweight even more.

From the standpoint of the model change, A2D improves the CTS accuracy and accelerates the model convergence by changing the neuron activation state of SNNs in the model training process. During training, the neural activity is expressed as the average firing probability per timestep per neuron (AFP). Most SNNs exhibit less than 0.10 AFP. A2D makes the firing probability higher in the early training stage and lower in the late training stage as shown in Figure 3(d), meaning the model will be more activated at the start of training. This accelerates the network convergence: A2D improves the accuracy over random training order with the
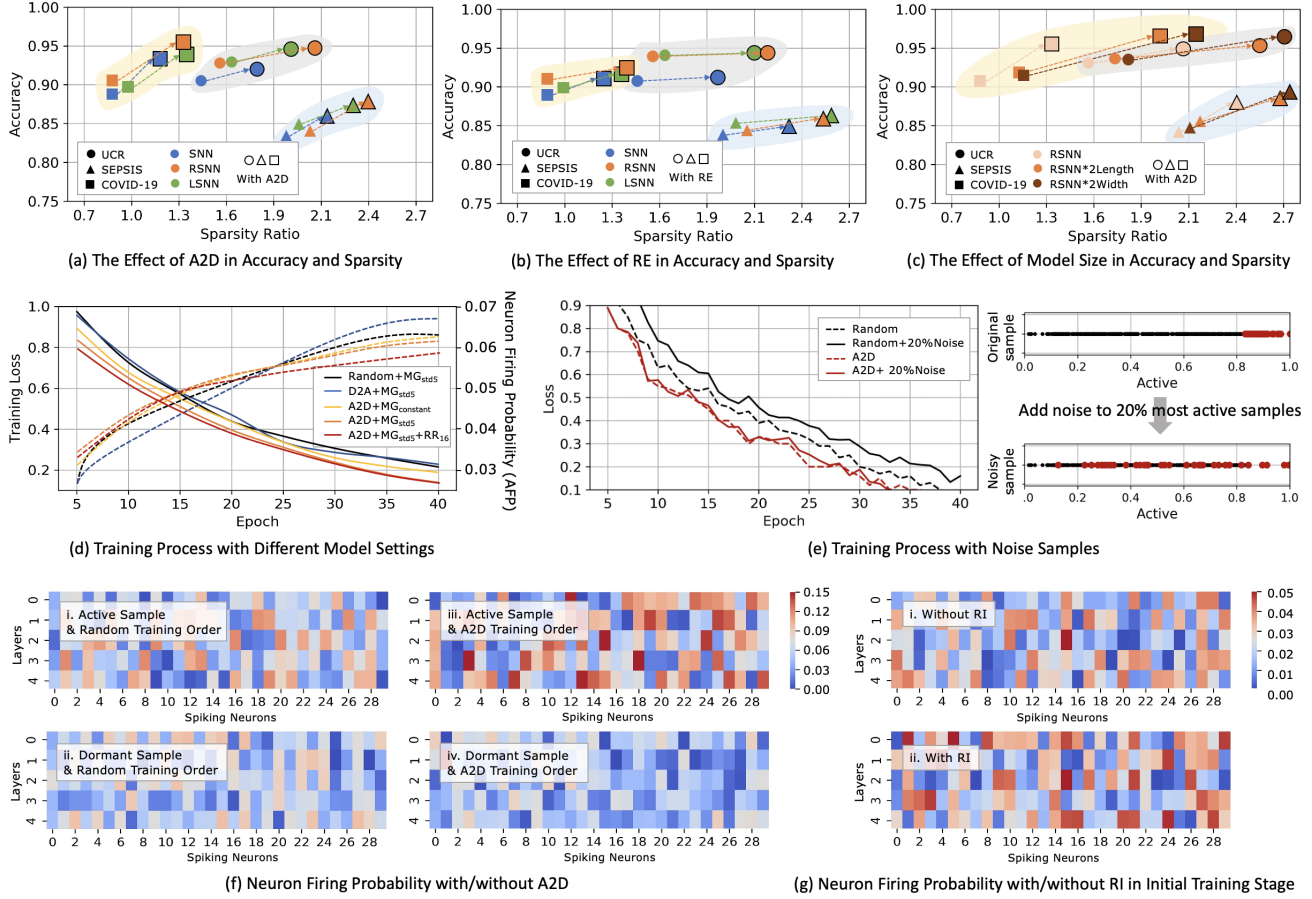
(a) The Effect of A2D in Accuracy and Sparsity

(b) The Effect of RE in Accuracy and Sparsity

(c) The Effect of Model Size in Accuracy and Sparsity

(d) Training Process with Different Model Settings

(e) Training Process with Noise Samples

(f) Neuron Firing Probability with/without A2D

(g) Neuron Firing Probability with/without RI in Initial Training Stage

Figure 3. Improvements in Model Sparsity, Firing Statutes, Convergence Process, and Anti-noise Performance after Using CSNN

same number of training epochs. While this is happening, wider networks make the phenomenon more obvious.

From the standpoint of the sample activity, A2D improves CTS accuracy by increasing neuron firing probability when inputting the active samples and decreases that when inputting the dormant samples compared with the random training order as shown in Figure 3(f). On the one hand, it can increase the network's initial convergence speed and, on the other hand, can lessen the network's exposure to noise data by treating noise data as dormant samples.

A2D gives SRNN a specific anti-noise ability as shown in Figure 3(e). We add Gaussian noise with a signal-to-noise ratio of 20db to the most 20% active TS samples in A2D. After recalculating the activity, these noisy samples become less active and the priority of participating in training is reduced. During training process, the impact of noise on SRNN's loss is significantly reduced after using A2D.

THE POWER OF VALUE-BASED REGIONAL ENCODING MECHANISM (RE)

The CTS accuracy of SNNs with RE is more accurate than that of SNNs without RE (The black lines of SNN+RE, RSNN+RE, and LSNN+RE are above the black lines of SNN, RSNN, and LSNN) as shown in Figure 2(d)-(f). Meanwhile, when using RE, A2D will affect SNNs more positively (The orange rectangle of SNNs+RE is bigger than green rectangle of SNNs), and anti-curriculum D2A will affect SNNs less negatively (The blue rectangle of SNNs+RE is smaller than the blue rectangle of SNNs).

RE can increase the sparsity ratio of SNNs more than A2D, although it does not enhance accuracy as much, shown in Figure 3(b). RE can also accelerate model convergence by increasing the neuron activity in the initial model training stage as shown in Figure 3(g).

RE works better with univariate TS than it does with multivariate TS as shown in Figure 2(d)-(f). For example, compared to the multivariate SEPSIS and COVID-19 datasets, the accuracy improvement in the univariate UCR dataset is greater (The lifting between the black line of SNNs+RE and

that of SNNs in (d) is greater than that in (e) and (f)). This might be because the region division criterion for multivariate TS is based on the mean value of all univariate, which may result in a lesser distinction between regions.

5. Conclusion

This paper investigates the power of curriculum learning (CL) on spiking neural networks (SNNs) for the classification of time series (CTS) for the first time. We design a curriculum for SNNs (`CSNN`) by proposing an active-to-dormant training order mechanism (`A2D`) and a value-based regional encoding mechanism (`RE`). Through the theoretical analysis and experimental confirmation, we reach the following results: The constructed SNNs have a greater potential for modeling TS data than ANNs. Because each neuron is a recursive system, it can represent the real-world irregularly-sampled TS without the need for any additional mechanisms; Compared to ANNs, CL affects SNNs and wider SNN structures more positively, whereas the anti-curriculum may affect SNNs negatively; The designed SNNs' curriculum `CSNN` can simulate the order of human knowledge acquisition and how the brain processes sequential input. It is appropriate for the properties of spiking neurons. By adjusting the spiking neuron firing statutes and activities, `CSNN` can improve the CTS accuracy, model convergence speed, network sparsity, and anti-noise ability of SNNs.

References

Bellec, G., Salaj, D., Subramoney, A., Legenstein, R., and Maass, W. Long short-term memory and learning-to-learn in networks of spiking neurons. In *Advances in Neural Information Processing Systems (NeurIPS)*, volume 31, pp. 795–805, 2018.

Castells, T., Weinzaepfel, P., and Revaud, J. Superloss: A generic loss for robust curriculum learning. In *Advances in Neural Information Processing Systems (NeurIPS)*, volume 33, 2020.

Chen, Y., Yu, Z., Fang, W., Ma, Z., Huang, T., and Tian, Y. State transition of dendritic spines improves learning of sparse spiking neural networks. In *International Conference on Machine Learning (ICML)*, volume 162, pp. 3701–3715, 2022.

Dau, H. A., Bagnall, A., Kamgar, K., Yeh, C.-C. M., Zhu, Y., Gharghabi, S., Ratanamahatana, C. A., and Keogh, E. The ucr time series archive. *IEEE/CAA Journal of Automatica Sinica*, 6(6):1293–1305, 2019. doi: 10.1109/JAS.2019.1911747.

Dz, A., Yi, Z., and Yang, L. Backeisnn: A deep spiking neural network with adaptive self-feedback and balanced excitatory–inhibitory neurons. *Neural Networks*, 154: 68–77, 2022. doi: 10.1016/j.neunet.2022.06.036.

Fang, H., Shrestha, A., and Qiu, Q. Multivariate time series classification using spiking neural networks. In *International Joint Conference on Neural Networks (IJCNN)*, pp. 1–7, 2020. doi: 10.1109/IJCNN48605.2020.9206751.

Fawaz, H. I., Forestier, G., Weber, J., Idoumghar, L., and Muller, P. Deep learning for time series classification: a review. *Data Mining and Knowledge Discovery*, 33(4): 917–963, 2019. doi: 10.1007/s10618-019-00619-1.

Gütig, R. and Sompolinsky, H. The tempotron: a neuron that learns spike timing–based decisions. *Nature Neuroscience*, 9:420–428, 2006. doi: 10.1038/nn1643.

Hacohen, G. and Weinshall, D. On the power of curriculum learning in training deep networks. In *International Conference on Machine Learning (ICML)*, volume 97, pp. 2535–2544, 2019.

Jiang, H., Li, Z., and Li, Q. Approximation theory of convolutional architectures for time series modelling. In Meila, M. and Zhang, T. (eds.), *International Conference on Machine Learning (ICML)*, volume 139, pp. 4961–4970, 2021.

Kheradpisheh, S. R. and Masquelier, T. Temporal backpropagation for spiking neural networks with one spike per neuron. *International Journal Of Neural Systems*, 30(6): 2050027, 2020. doi: 10.1142/S0129065720500276.

Lin, J., Chen, Q., Zhou, J., Jin, J., and He, L. CUP: curriculum learning based prompt tuning for implicit event argument extraction. In *International Joint Conference on Artificial Intelligence (IJCAI)*, pp. 4245–4251, 2022. doi: 10.24963/ijcai.2022/589.

Reyna, M. A., Josef, C., Seyedi, S., and Jeter, R. Early prediction of sepsis from clinical data: the physionet/computing in cardiology challenge 2019. In *Computing in Cardiology Conference (CinC)*, pp. 1–4, 2019. doi: 10.22489/CinC.2019.412.

Seymour, C. W., Gesten, F., and Prescott, H. C. Time to treatment and mortality during mandated emergency care for sepsis. *New England Journal of Medicine*, 376(23): 2235–2244, 2017. doi: 10.1056/NEJMOA1703058.

Sun, C., Hong, S., Song, M., and Li, H. A review of deep learning methods for irregularly sampled medical time series data. *CoRR*, abs/2010.12493, 2020a.

Sun, C., Hong, S., Song, M., Li, H., and Wang, Z. Predicting covid-19 disease progression and patient outcomes based on temporal deep learning. *BMC Medical Informatics and Decision Making*, 21:45, 2020b. doi: 10.1186/s12911-020-01359-9.

Sun, C., Hong, S., Song, M., and Li, H. Te-esn: Time encoding echo state network for prediction based on irregularly sampled time series data. In *International Joint Conference on Artificial Intelligence (IJCAI)*, pp. 3010–3016, 2021. doi: 10.24963/ijcai.2021/414.

Sun, C., Song, M., Cai, D., Zhang, B., Hong, S., and Li, H. Confidence-guided learning process for continuous classification of time series. In *International Conference on Information & Knowledge Management (CIKM)*, pp. 4525–4529, 2022. doi: 10.1145/3511808.3557565.

Tian, G., Huang, T., and Wu, S. Excitation-inhibition balanced spiking neural networks for fast information processing. In *IEEE International Conference on Systems, Man and Cybernetics (SMC)*, pp. 249–252, 2019. doi: 10.1109/SMC.2019.8914566.

Torab, P. and Kamen, E. W. On approximate renewal models for the superposition of renewal processes. In *IEEE International Conference on Communications (ICC)*, pp. 2901–2906, 2001. doi: 10.1109/ICC.2001.936680.

Xie, Y., Hu, P., Li, J., Chen, J., Song, W., Wang, X.-J., Yang, T., Dehaene, S., Tang, S., Min, B., and Wang, L. Geometry of sequence working memory in macaque prefrontal cortex. *Science*, 375(6581):632–639, 2022. doi: 10.1126/science.abm0204.

Yan, L., Zhang, H.-T., Goncalves, J., Xiao, Y., Wang, M., Guo, Y., Sun, C., Tang, X., Jing, L., Zhang, M., et al. An interpretable mortality prediction model for covid-19 patients. *Nature Machine Intelligence*, 2:283–288, 2020. doi: 10.1038/s42256-020-0180-7.

Yin, B., Corradi, F., and Bohté, S. M. Accurate and efficient time-domain classification with adaptive spiking recurrent neural networks. *Nature Machine Intelligence*, 3: 905–913, 2021. doi: 10.1101/2021.03.22.436372.

Zerveas, G., Jayaraman, S., Patel, D., Bhamidipaty, A., and Eickhoff, C. A transformer-based framework for multivariate time series representation learning. In *ACM SIGKDD Conference on Knowledge Discovery & Data Mining (KDD)*, pp. 2114–2124, 2021. doi: 10.1145/3447548.3467401.

Zhang, T., Cheng, X., Jia, S., ming Poo, M., Zeng, Y., and Xu, B. Self-backpropagation of synaptic modifications elevates the efficiency of spiking and artificial neural networks. *Science Advances*, 7(43):eabh0146, 2021. doi: 10.1126/sciadv.abh0146.

Zhao, J., Huang, F., Lv, J., Duan, Y., Qin, Z., Li, G., and Tian, G. Do RNN and LSTM have long memory? In *International Conference on Machine Learning (ICML)*, volume 119, pp. 11365–11375, 2020.

A. Theorems, Propositions, and Proofs

Theorem 1. *In SNN, different input orders of spike trains make the neuron output different spike trains.*

Proof. We assume two input spike trains with the same spike number and equal time intervals, most simply, an l-length all-one spike sequence $S_0 = (1)^l$, and an l-length half-one spike sequence $S_1 = (0)^{\frac{l}{2}} \wedge (1)^{\frac{l}{2}}$. When the SNN training starts, the parameters w are initialized randomly under a Gaussian distribution $\mathcal{N}(\mu, \sigma^2)$. We focus on the membrane potential v of one neuron of the first layer and assume $\frac{\mu}{2} < V_{th} < \mu$.

If the learning order is $S_0 \rightarrow S_1$: After inputting S_0, the membrane potential is $v = \sum_{i=1}^{l} w\text{PSP} \approx \mu > V_{th}$, then the neuron fires and $w \rightarrow w'$; After inputting S_1, $v \approx \frac{\mu'}{2}$.

If the learning order is $S_1 \rightarrow S_0$: After inputting S_1, $v \approx \frac{\mu}{2} < V_{th}$, then the neuron does not fire and w remains; After inputting S_0, $v \approx \mu > V_{th}$, then the neuron fires.

When $\frac{\mu'}{2} > V_{th}$, there will be two fires in the first case but one in the second case $O_0 = (1,1) \neq O_1 = (0,1)$. $\square$

Theorem 2. *The difference between objectives $\mathcal{U}_p$ and $\mathcal{U}$, which are computed with and without curriculum prior p, is the covariance between U_ϑ and p.*

$$\mathcal{U}_p(\vartheta) = \mathcal{U}(\vartheta) + \hat{\text{Cov}}[U_\vartheta, p]$$

Proof. By deforming the objective $\mathcal{U}_p(\vartheta) = \hat{\mathbb{E}}_p[U_\vartheta] = \sum_{i=1}^{N} U_\vartheta(X_i)p(X_i)$, we can find that $\mathcal{U}_p(\vartheta)$ is determined by the correlation between $U_\vartheta(X)$ and $p(X)$.

$$
\begin{aligned}
\mathcal{U}_p(\vartheta) &= \sum_{i=1}^{N} U_\vartheta(X_i)p(X_i) \\
&= \sum_{i=1}^{N} U_\vartheta(X_i)p(X_i) - 2N\hat{\mathbb{E}}(U_\vartheta)\hat{\mathbb{E}}(p) + 2N\hat{\mathbb{E}}(U_\vartheta)\hat{\mathbb{E}}(p) \\
&= (\sum_{i=1}^{N} U_\vartheta(X_i)p(X_i) - N\hat{\mathbb{E}}(p)\sum_{i=1}^{N} U_\vartheta(X_i) \\
&\quad - N\hat{\mathbb{E}}(U_\vartheta)\sum_{i=1}^{N} p(X_i) + N\hat{\mathbb{E}}(U_\vartheta)\hat{\mathbb{E}}(p)) + N\hat{\mathbb{E}}(U_\vartheta)\hat{\mathbb{E}}(p) \\
&= \sum_{i=1}^{N} (U_\vartheta(X_i) - \hat{\mathbb{E}}[U_\vartheta])(p_i - \hat{\mathbb{E}}[p]) + N\hat{\mathbb{E}}(U_\vartheta)\hat{\mathbb{E}}(p) \\
&= \hat{\text{Cov}}[U_\vartheta, p] + \mathcal{U}(\vartheta)
\end{aligned}
$$

$\square$

Theorem 3. *Curriculum learning changes the optimization function from $\mathcal{U}(\vartheta)$ to $\mathcal{U}_p(\vartheta)$. The optimal $\tilde{\vartheta}$ maximizes the covariance between p and $U_{\tilde{\vartheta}}$:*

$$\tilde{\vartheta} = \arg\max_\vartheta \mathcal{U}(\vartheta) = \arg\max_\vartheta \hat{\text{Cov}}[U_\vartheta, p]$$

and satisfying two claims:

$$\tilde{\vartheta} = \arg\max_\vartheta \mathcal{U}(\vartheta) = \arg\max_\vartheta \mathcal{U}_p(\vartheta)$$

$$\forall \vartheta \quad \mathcal{U}_p(\tilde{\vartheta}) - \mathcal{U}_p(\vartheta) \geq \mathcal{U}(\tilde{\vartheta}) - \mathcal{U}(\vartheta)$$

Proof. For claim 2, from Theorem 2,

$$
\begin{aligned}
\mathcal{U}_p(\tilde{\vartheta}) - \mathcal{U}_p(\vartheta) &= \mathcal{U}_p(\tilde{\vartheta}) - \mathcal{U}(\vartheta) - \hat{\text{Cov}}[U_\vartheta, p] \\
&\geq \mathcal{U}_p(\tilde{\vartheta}) - \mathcal{U}(\vartheta) - \hat{\text{Cov}}[U_{\tilde{\vartheta}}, p] \\
&= \mathcal{U}(\tilde{\vartheta}) - \mathcal{U}(\vartheta)
\end{aligned}
$$

$\square$

Proposition 1. *When using the active-to-dormant training order, Theorem 3 holds if the variance of the maximum function is roughly constant in the relevant range of plausible parameter values.*

$$\mathcal{U}_p(\tilde{\vartheta}) - \mathcal{U}_p(\vartheta) \geq \mathcal{U}(\tilde{\vartheta}) - \mathcal{U}(\vartheta) \quad \forall \vartheta : \mathrm{Cov}[U_\vartheta, U_{\tilde{\vartheta}}] \leq \mathrm{Var}[U_{\tilde{\vartheta}}]$$

Proof. Based on Equation 11, $\mathcal{U}_p(\vartheta) = \mathcal{U}(\vartheta) + \frac{1}{P}\mathrm{Cov}[U_\vartheta, U_{\tilde{\vartheta}}]$. Then, at the optimal point $\tilde{\vartheta}$: $\mathcal{U}_p(\tilde{\vartheta}) = \mathcal{U}(\tilde{\vartheta}) + \frac{1}{P}\mathrm{Var}[U_{\tilde{\vartheta}}]$; at any other point: $\mathcal{U}_p(\vartheta) \leq \mathcal{U}(\tilde{\vartheta}) + \frac{1}{P}\sqrt{\mathrm{Var}[U_\vartheta]\mathrm{Var}[U_{\tilde{\vartheta}}]}$.

The sample itself is randomly distributed. Assuming a constant $b = \mathrm{Var}[U_\vartheta]$, Theorem 3 follows $\mathcal{U}_p(\vartheta) \leq \mathcal{U}(\tilde{\vartheta}) + \frac{b}{P} = \mathcal{U}_p(\tilde{\vartheta})$, i.e. $\tilde{\vartheta} = \arg\max_\vartheta \mathcal{U}_p(\vartheta)$. $\square$

Theorem 4. *The difference between the objective score with CL and that without CL will be greater if there is a larger score discrepancy between each sample.*

Proof. Without CL, since the training samples are fixed, $\mathrm{Var}[U_\vartheta]$ is constant; With CL, based on Equation 11, as $P \approx \mathbb{E}[e^{-L(X_i)}]$ is constant, $\mathrm{Var}[U_{\tilde{\vartheta}}] \propto \mathrm{Var}[p]$. Thus,

$$\mathrm{Var}[p] \uparrow \; \rightarrow \mathrm{Var}[U_{\tilde{\vartheta}}] \uparrow$$
$$\rightarrow \mathbb{E}[(U_\theta(X_i) - \mathbb{E}(U_\theta))(U_{\tilde{\vartheta}}(X_i) - \mathbb{E}(U_{\tilde{\vartheta}}))] \downarrow$$
$$\rightarrow \mathrm{Cov}[U_\vartheta, U_{\tilde{\vartheta}}] \downarrow$$

$\square$

Proposition 2. *The regional encoding mechanism contributes to SNNs' CL by increasing the variation of sample activity and assisting the model's quick response to input changes.*

Proof. At time t, we call spiking neurons with $x_t \in \mathcal{I}_m$ as excitatory neurons S_E and neurons with $x_t \notin \mathcal{I}_m$ as inhibitory neurons S_I. For S_I, the membrane potential is only discharged but not charged, i.e. Equation 2 only has the rightmost item. We can regard it as an extreme case of feed-forward and feed-back inhibition (Dz et al., 2022). The balance of excitation and inhibition can achieve fast-response to input changes (Tian et al., 2019).

Based on (Dz et al., 2022), the inhibition changes piking rate, the value of Equation 10 increases under the true class label, so that the difference among computed values of Equation 4 of samples with different labels becomes larger. Thus, $\mathrm{Var}[U_{\tilde{\vartheta}}]$ increases.

According to Equation 12, the neuronal input is given by external input and recurrent input $I_i[t] = I_i^{ext}[t] + I_i^{rec}[t]$. With a probability P_C, each neuron connecting the input layer receive inputs from $K_E = P_C \mathrm{S}_E$ excitatory neurons and $K_I = P_C \mathrm{S}_I$ inhibitory. The recurrent excitatory (inhibitory) input can be approximated by a Poisson process (Torab & Kamen, 2001). a Poisson presynaptic spike train is $I_i^{rec}[t] = \mu_i^{rec} + \sigma_i^{rec}\xi_i^{rec}$. Hereafter, we omit the neuron index i, and use the mpty subscript $e/i = E$ or I to denote whether the population is excitatory or inhibitory. $\mu_{e/i} = \mu_{rec,e/i} + f_{e/i}\mu_{ext}$, $\sigma_{e/i}^2 = \sigma_{ext}^2 + \sigma_{rec,e/i}^2$, and $\beta_{e/i} = \frac{\sigma_{e/i}^2}{\mu_{e/i}}$ are mean, variance, and variance-to-mean radio of the input received by a neuron. In reality, σ_{ext}^2 is usually very small and $\beta_{e/i}$ can be approximated as a constant irrespective to external inputs. Referring to the derivation process in (Tian et al., 2019), we directly draw a conclusion: The neural population firing rate is Equation 16. It linearly encodes the external input mean. Which ensures that the network's response to input changes is very fast.

$$r_{e/i} = \frac{\mu_{e/i}}{V_{th}V_0} \propto \mu_{ext} \tag{16}$$

$\square$